Pergamon

Journal of Atmospheric and Terrestrial Physics, Vol. 56, No. 6, pp. 755–774, 1994

0021–9169/94 $6.00 + .00

A statistical study of the structure, saturation and sources of inertio-gravity waves in the lower stratosphere observed with the MU radar

K. SATO

Department of Geophysics, Faculty of Science, Kyoto University, Kyoto 606-01, Japan

(*Received in final form* 19 *April* 1993; *accepted* 22 *April* 1993)

Abstract—Using wind data monitored by the MU radar at Shigaraki, Japan (35°N, 136°E) in the three years of 1986–1988, a statistical analysis is made of inertio-gravity waves (IGWs) with short vertical wavelengths ($\leqslant 4$ km) and long ground-based periods ($\geqslant 10$ h) which are dominant in the lower stratosphere in all seasons. The intensity of the IGWs is at its peak in winter when a strong subtropical westerly wind jet is situated over Japan. The zonal component of vertical momentum flux associated with the IGWs in winter is mostly negative and the magnitude decreases with altitude, suggesting a strong interaction between IGWs and the background wind field.

The parameters of the wave structure are estimated by a hodograph analysis, taking into consideration the effect of vertical shear of the background wind that is not negligible in winter. The obtained parameters, such as the vertical and horizontal energy propagation directions, vertical and horizontal wavelengths, and intrinsic period, are compared between two periods with a strong subtropical jet including winter and with a weak jet including summer. The degree of saturation of IGWs, defined as the ratio of amplitude of the horizontal perturbation velocity parallel to the horizontal wavenumber vector to the intrinsic horizontal phase velocity, is also statistically and directly examined using the results of wave parameter estimation. It is shown that the degree of saturation is larger in winter than in summer and that there are few oversaturated IGWs even in winter.

Moreover, in order to examine the generation mechanisms of the IGWs, an analysis is made from two points of view: geostrophic adjustment of the westerly wind jet and the topographic effect. The meridional propagation direction of IGWs is examined in a section of latitude and altitude relative to the jet axis using ECMWF operational data. Most of the IGWs observed in the 12–18 km height region (above the ground) in winter propagate meridionally toward the jet axis, indicating that geostrophic adjustment at least just as the jet axis is not the main generation mechanism of the IGWs. On the other hand, the characteristics of intensive IGWs propagating westward relative to the background wind in the 18–22 km height region in winter are in good accord with mountain waves excited in strong westerly winds near the surface.

1. INTRODUCTION

Fine wavelike structures with short vertical wavelengths ($\leqslant 3$ km) and long periods ($\geqslant 10$ h) in the lower stratosphere have been known through continuous wind observations with fine vertical resolution: for example, by the recently developed MST (mesosphere stratosphere and troposphere) radar at Arecibo, Puerto Rico (18.4°N, 66.8°W) (SATO and WOODMAN, 1982; CORNISH and LARSEN, 1989) and by tracing balloons at a tropical location in the Atlantic Ocean (8.5°N, 23.5°W) (CADET and TEITELBAUM, 1979). Through theoretical considerations these wavelike structures are found to be due to inertio-gravity waves (IGWs). Similar small-scale wind structures lasting a long time have been observed also by the MU radar (an MST radar) at Shigaraki, Shiga, Japan (34.9°N, 136.1°E) in the lower stratosphere in all seasons. There are several case studies showing evidence of IGWs for the wavy structure by HIROTA and NIKI (1986), FRITTS *et al.* (1988), YAMANAKA *et al.* (1989), and USHIMARU and TANAKA (1990).

The main purpose of this study is to describe the statistical characteristics of IGWs in the lower stratosphere in terms of wave structure and intensity, and to examine the source mechanisms, using routinely monitored wind data obtained by the MU radar in the three years of 1986–1988.

Previous statistical studies on gravity waves are briefly reviewed in the following. For the seasonal variation of gravity wave intensity as a function of latitude, there was a pioneering work by HIROTA (1984) for the stratosphere (25–65 km) using rocket data. He showed that an annual cycle with the maximum in winter is dominant in middle and high latitudes, while in low latitudes a semiannual cycle with the maxima around the equinoxes is distinct. For middle latitudes, the seasonal variation has been

elucidated also as a function of altitude throughout the middle atmosphere, by synthesizing the previous statistical studies for each part of the height region using data provided by radiosondes, MST radars, and lidars. In the lower stratosphere (~15–25 km), an annual cycle is observed with the maximum in winter (KITAMURA and HIROTA, 1989; MURAYAMA *et al.*, 1993). The annual cycle is dominant up to a height of about 60 km whereas a second weak peak appears in summer above that height in the lower mesosphere (WILSON *et al.*, 1991). The semiannual variation is clearer in the middle and upper mesosphere and lower thermosphere and the summer peak rather dominates over the winter one (MANSON and MEEK, 1986; EBEL *et al.*, 1987; VINCENT and FRITTS, 1987; TSUDA *et al.*, 1990). In order to obtain a comprehensive interpretation of the nature of gravity waves in the middle atmosphere, the propagation properties and sources of gravity waves in each height region need to be examined.

In the lower stratosphere, a lot of IGWs propagating meridionally were reported by several case studies (e.g. HIROTA and NIKI, 1986; YAMANAKA *et al.*, 1989). On the basis of this fact, geostrophic adjustment of the subtropical westerly wind jet is considered to be an important generation mechanism of IGWs in the lower stratosphere of middle latitudes. The possibility was examined by FRITTS and LUO (1992) and LUO and FRITTS (1993) using two- and three-dimensional numerical models, respectively. A statistical study by KITAMURA and HIROTA (1989) using radiosonde data, which cover a similar altitude and geographical region to this study, showed a number of gravity waves propagating northwestward away from the westerly wind jet. The intensity of the gravity waves had its maximum in winter when a strong jet existed. These facts support the possibility of the geostrophic adjustment process.

However, the correlation between the intensities of gravity waves and the subtropical jet is recognized only on a seasonal time-scale. A detailed analysis of IGWs is needed, restricted to seasons with a strong subtropical jet. In this study, taking the latitude of the MU radar site relative to the jet axis as a parameter with the aid of the operational analysis by European Centre for Medium-range Weather Forecasts (ECMWF), the characteristics of IGWs are examined.

Another important generation mechanism of gravity waves is the topographic effect. HINES (1988) showed the possibility of topographically forced gravity waves (mountain waves) for the wavelike wind structure observed at Arecibo by SATO and WOODMAN (1982). Mountain waves have often been observed at Shigaraki in vertical wind disturbances from late autumn to early spring (SATO, 1990), which is also coincident with the strong subtropical jet. This paper examines the possibility of mountain waves for some of the IGWs observed by the MU radar.

In the next section, a description of the MU radar data is given and a criterion for extracting IGWs from the original data is shown. Section 3 gives statistics for the intensity and wave parameters of the IGWs and describes the difference between summer and winter. Section 4 focuses on generation mechanisms of the IGWs. Discussion is presented in Section 5. The results are summarized and concluding remarks are given in Section 6.

2. DATA DESCRIPTION AND EXTRACTION OF IGWs

Analyzed are the data obtained by routine wind observations made by the MU radar for 100 h every month in the three years of 1986–1988. Since the observations in December 1986 were missing, data obtained in December 1985 are used in place of it. One-minute observations of winds were made about every 2.5 min by five beams directed vertically and tilted to the north, south, east, and west with a zenith angle θ of 10°. The observed height region is 5–24 km with a resolution of 150 m along the beam directions, while the top of region where the wind data are available depends on the atmospheric conditions. It is noted that the MU radar site is 370 m above sea level, and that all altitudes described in this paper are above the ground level. A detailed description of the MU radar was given by FUKAO *et al.* (1985a, b).

Figure 1 shows typical time series of the vertical profile of the zonal wind component in winter (December 1985) and in summer (July 1986). Wavelike structures with vertical wavelengths of 1–3 km lasting a long time (>10 h) are clearly seen above the jet peak in both observation periods. These are considered to be due to IGWs from the previous case studies. Since the time interval of monitoring is not constant through the three years and the wave periods of the IGWs are much longer than 1 h as found from Fig. 1, the original wind data were reduced by averaging for 30 min.

Vertical wavenumber (m) spectra of the horizontal wind fluctuations in the middle atmosphere have a shape of m^{-3} in a region of $m \geq m_*$, where m_* is the characteristic wavenumber, while the spectral slope is much gentler at smaller ms (e.g. SMITH *et al.*, 1987). This spectral shape indicates the dominance of waves having wavenumbers near m_*. Estimation of m_* could not be made in this study because the observed height

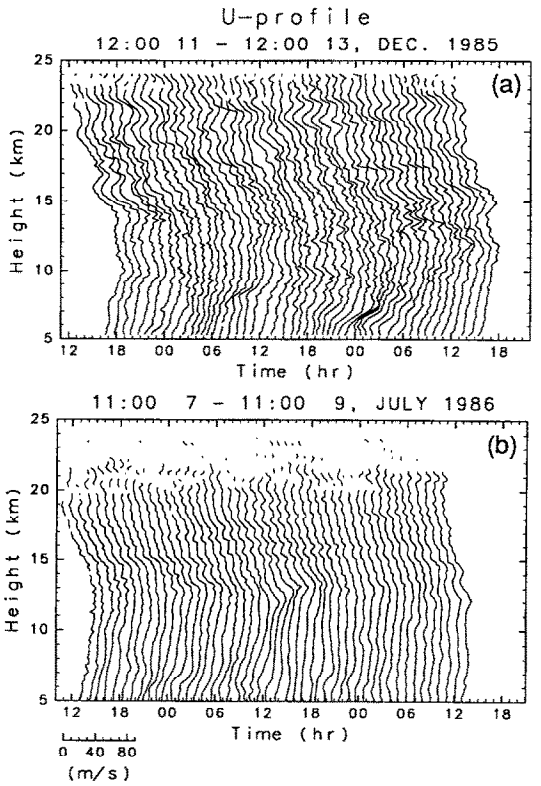

Fig. 1. Typical examples of the time series of 1-h averaged vertical profile of the horizontal wind component observed by the MU radar in (a) winter and (b) summer. Scale of the horizontal wind is shown at the bottom. The profiles are shifted by an interval of 10 m s^{-1}.

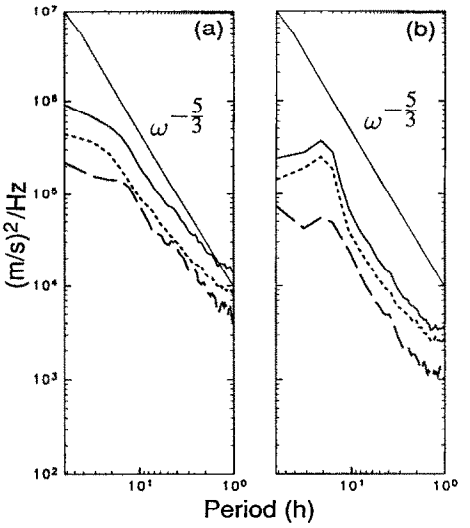

Fig. 2. Power spectra of the zonal wind fluctuations averaged for (a) winter and (b) summer. The dotted and dashed curves show the spectra with vertical wavelengths shorter than 4 km and longer than 4 km, respectively, and the solid curves show the total.

region was not always sufficiently extended in the lower stratosphere for the spectral calculation. According to the statistical study by TSUDA *et al.* (1991), using data of radiosondes launched at the MU radar site, the vertical wavelength corresponding to m_* for temperature fluctuations, which is equal to that for horizontal wind fluctuations theoretically, is about 2 km in the lower stratosphere. This vertical wavelength accords well with those of the IGWs in Fig. 1. Hence a highpass filter with a cutoff wavelength of 4 km is used in order to extract IGW components from the original vertical profiles.

Frequency power spectra of horizontal wind fluctuations are obtained to examine the dominant wave periods of IGWs. The spectrum of the time series at each altitude is obtained and averaged for the altitude region from 16 to 22 km in the lower stratosphere. Figure 2(a) and 2(b) shows the spectra averaged for winter (December, January and February) and summer (June, July and August), respectively. The dotted and dashed curves show the spectra for wind fluctuations with vertical wavelengths shorter and larger than 4 km, respectively, and the solid curves show the spectra for all fluctuation components. The characteristics seen in the spectra are similar in both seasons. The level of the spectrum for the short vertical wavelength component including IGWs is higher than that for the long vertical wavelength component. The discrepancy is extremely large in periods longer than about 10 h. This feature shows the existence of a spectral peak in the two-dimensional space of vertical wavenumber and frequency, corresponding to the IGWs. Therefore the IGW components are defined as components having vertical wavelengths shorter than 4 km and periods longer than 10 h, independently of the season, although the spectral peak is more distinct in the summer spectra than in the winter ones. Note that broad bandwidths both in vertical wavenumber and frequency are taken for the definition of IGW components, since closer estimation of the frequency and vertical wavelength by the method of least squares will be made in the next section.

Zonal, meridional, and vertical wind profiles of the IGW components are plotted in Fig. 3 for the same observation period as Fig. 1(a). Wavelike structures are observed in both the meridional and vertical perturbation velocities as well as in the zonal one. This is also the case for the summer profile corresponding

to Fig. 1(b) (not shown). The accuracy of the line-of-sight wind velocity estimation by the original 1-min observation is about 0.1 m s^{-1} (YAMAMOTO *et al.*, 1988). The lowpass filtering process for extracting the IGW components, roughly corresponding to a running mean of 100 data points (~5 h), reduces the estimation error in the line-of-sight wind velocity to about 0.01 m s^{-1}. Since the vertical wind component is obtained directly using the vertical beam, its error for IGWs is about 0.01 m s^{-1}. The errors in the zonal and meridional perturbation velocities of IGWs, which are obtained using the line-of-sight velocities of the oblique beams, are roughly estimated to be about 0.06 m s^{-1} by multiplying the line-of-sight velocity error of 0.01 m s^{-1} by a factor of $(\sin\theta)^{-1} = 5.76$. The amplitudes of the wavelike structures observed both in winter (Fig. 3) and in summer (not shown) are much larger than these estimation errors. The examination of the characteristics of IGWs is, therefore, meaningful.

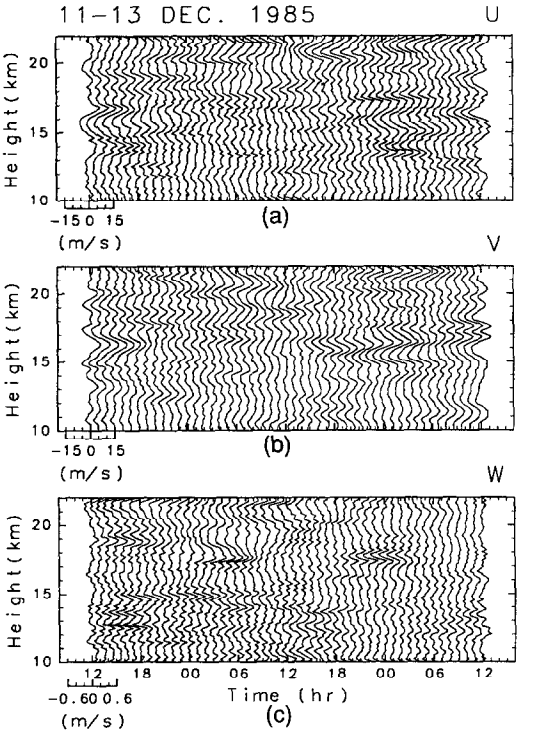

Fig. 3. Time series of the (a) zonal, (b) meridional, and (c) vertical perturbation velocities of the IGWs extracted using a lowpass filter in time with a cutoff period of 10 h and a highpass filter in vertical with a cutoff length of 4 km for the same observation period of Fig. 2(a).

3. STATISTICAL CHARACTERISTICS OF IGWs

3.1. *Seasonal variation of intensity of IGWs and vertical momentum flux*

Figure 4 shows the zonal ($\overline{u'w'}$) and meridional ($\overline{v'w'}$) components of vertical momentum flux, the variance of horizontal perturbation velocities ($\overline{u'^2+v'^2}$), and the anisotropy ($100\times\overline{u'^2}/\overline{u'^2+v'^2}$) of the IGWs, together with the strength of the subtropical jet (V_{max}) over the MU radar site as a function of month. Here, u', v', and w' denote the zonal, meridional, and vertical perturbation velocities of the IGWs, respectively. The variance and momentum flux were estimated for the entire observation period of each month and the 16–22 km height region. The jet strength V_{max} is plotted as the maximum of the background horizontal wind in the vertical profile obtained by averaging unfiltered data for each month. The altitude of the background wind maximum is 11–12 km every month. Estimation was made only when the number of available data was more than 50% of the total. Different marks denote different years and the solid curve traces the average for each month. The error in the vertical momentum flux is about 1×10^{-3} m s^{-1}. A detailed desciption of the error estimation is given in the Appendix.

It is found that an annual cycle is dominant in the time series of $\overline{u'^2+v'^2}$ with a maximum in winter while a secondary maximum is observed in April, which is consistent with the result of KITAMURA and HIROTA (1989). The meridional wind variance $\overline{v'^2}$ is always slightly larger than $\overline{u'^2}$. The magnitude of the zonal component of vertical momentum flux $\overline{u'w'}$ shows a similar variation to the variance, and $\overline{u'w'}$ is mostly negative in winter and almost zero in summer. The meridional component $\overline{v'w'}$ is biased also toward negative but relatively weak values and the annual cycle is not clear. The magnitude of $\overline{u'w'}$ is several tens of percent of that due to severe mountain waves (LILLY and KENNEDY, 1973; SATO, 1990) and due to gravity waves associated with a typhoon (SATO, 1993). The vertical momentum flux should be regarded as significantly larger, however, since the IGWs have *always* been observed, though this is not the case for typhoons.

MURAYAMA *et al.* (1993) analyzed the variance and momentum flux of *all* gravity wave components having ground-based frequencies between the Brunt Väisälä and inertial frequencies using the same MU radar data as used in this study. The characteristics shown in their study accord well with the above results in both magnitude and sign. This means that the IGWs analyzed in this study are dominant and important waves in the lower stratosphere.

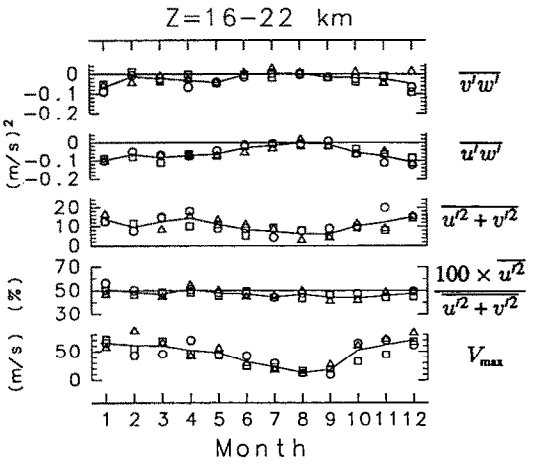

Fig. 4. The zonal and meridional components of vertical momentum flux associated IGWs ($\overline{u'w'}$ and $\overline{v'w'}$, respectively) and variance of the horizontal perturbation velocities of IGWs ($\overline{u'^2+v'^2}$) and contribution of the zonal perturbation velocity to the variances $[(100\times\overline{u'^2})/(\overline{u'^2+v'^2})]$, and the maximum of the horizontal wind averaged for each observation time (V_{max}), as a function of month. The circles, squares, and triangles show the data in 1986, 1987, and 1988, respectively.

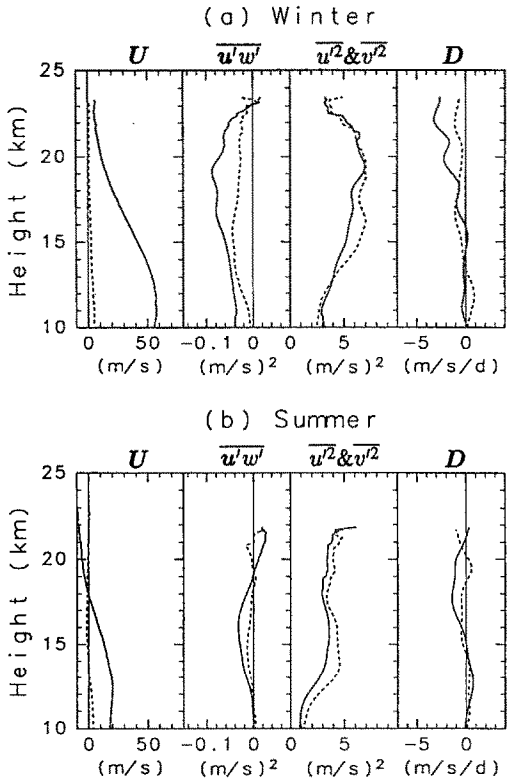

Fig. 5. Vertical profiles of the background wind (U), vertical momentum flux $\overline{u'w'}$, variance of the horizontal wind fluctuations ($\overline{u'^2}$ and $\overline{v'^2}$), and the drag (D) calculated from the vertical profile of vertical momentum flux, in (a) winter and (b) summer. The solid and dotted lines show the zonal and meridional components, respectively.

A strong subtropical westerly jet stream is located over the MU radar site. The time series of the jet strength has a similar annual cycle with a maximum in winter to the IGW variance (Fig. 4), suggesting that IGWs in the lower stratosphere are related to the subtropical jet. Further examination is made by comparing two seasons divided according to the strength of the subtropical jet. We define months with a strong jet, October through May, as winter and the other months with a weak jet as summer.

Vertical profiles of the background wind, vertical momentum flux, variance, and drag to the background wind averaged for winter and summer months are shown in Fig. 5. The drag $\boldsymbol{D}$ is calculated from the vertical profile of vertical momentum flux using

$$\boldsymbol{D} = -\frac{1}{\rho_0(z)}\frac{\mathrm{d}\rho_0(z)\overline{\boldsymbol{u}'w'}}{\mathrm{d}z}, \qquad (1)$$

where $\rho_0(z)$ is the air density adopted from the U.S. Standard Atmosphere 1976, which shows a representative profile in the mid-latitudes and does not cause significant error for the examination of this study restricted to the lower stratosphere.

The solid and dotted curves show the zonal and meridional components of each quantity, respectively. In winter $\overline{u'^2}$ has a peak around a height of 20 km while $\overline{v'^2}$ has two peaks at 16 and 20 km. This suggests that there are two dominant waves around 16 km and around 20 km, and that the characteristics of the two waves are different. The magnitude of the zonal component of vertical momentum flux $\overline{u'w'}$ is larger than the meridional one in winter and decreases above a height of 20 km where the background horizontal wind is very weak. The zonal component of drag due to the convergence of $\overline{u'w'}$ is negative and large above 20 km.

On the other hand in summer all quantities are smaller than those in winter. An interesting feature is that the sign of $\overline{u'w'}$ changes once around a height of 19 km where the background zonal wind profile crosses the zero line. Since the error in $\overline{u'w'}$ is of the order of 1×10^{-3} m^2 s^{-3} as shown in the Appendix, the vertical profile of $\overline{u'w'}$ is continuous, and the sign reversal of $\overline{u'w'}$ is observed in every vertical profile of each month belonging to summer (not shown), this feature is considered to be statistically meaningful. Such a change in sign of vertical momentum flux is

not explained by the vertical propagation of one wave. The zonal component of drag estimated from the profile of vertical momentum flux is also negative but not so large as in winter.

Note that the positive sign of $\overline{u'w'}$ around 21 km in summer is the same as the estimation for the mesosphere using the MU radar data by TSUDA *et al.* (1990) although the density-weighted magnitude of $\overline{u'w'}$ ($\sim 2\times10^{-3}$ kg m^{-1} s^{-2}) is 20 times larger than in the mesosphere ($\sim 1\times10^{-4}$ kg m^{-1} s^{-2} at a height of 70 km), indicating that significant convergence of the zonal momentum flux must occur between the lower stratosphere and the mesosphere in summer. On the other hand in winter in the mesosphere, the sign of $\overline{u'w'}$ is negative but the density-weighted magnitude is too small ($\sim -5\times10^{-5}$ kg m^{-1} s^{-2} at 70 km) for detection by the MU radar in the lower stratosphere. In such a sense, the almost zero value of $\overline{u'w'}$ observed around the top altitude of 23 km in Fig. 5 is compatible with the $\overline{u'w'}$ in the mesosphere. However, further discussion cannot be made for winter. The positive sign of $\overline{u'w'}$ in winter around 23 km may not be as statistically reliable as in summer because the magnitude is small and positive values are observed at only a few data points in height.

PALMER *et al.* (1986) showed that serious systematic errors in the general circulation models (GCMs) such as a poleward shift of the subtropical westerly jet and excessive strength of the westerly wind in the lower stratosphere are alleviated by including gravity wave drag. The drag obtained in this study (1.5–2.5 m s^{-1} day^{-1}) is almost equal to the quantity required to reduce the systematic errors in GCMs (e.g. IWASAKI *et al.*, 1989). This fact reconfirms the importance of gravity wave drag in the lower stratosphere and assures validity of the magnitude of the drag used in the parameterization scheme of GCMs.

3.2. *Hodograph analysis*

Parameters describing the wave structure of vertical and horizontal wavelengths, intrinsic frequency, and propagation direction are estimated by analyzing hodographs, i.e. the vertical variation of the horizontal wind vector of IGWs. The hodograph for every height region of 1.65 km (11 data points) in each vertical profile of the IGW component at an interval of 30 min was fitted to an ellipse using the method of least squares. A linear fitting with a fixed vertical wavelength $\lambda_z(=2\pi/m)$ was performed so that the results were stable. Among 31 fittings having different λ_z in a range of 1.5–4.5 km with an interval of 0.1 km, optimal parameters with the least residual were obtained. Wave parameters were estimated only when the variance due to the elliptic wind components was larger than twice that of the residual, the ratio of the short to long axis of the ellipse was less than 0.9, and the amplitude of the horizontal perturbation velocity in the direction of the long axis exceeded 1 m s^{-1}. This method is effective for the parameter estimation of those IGWs whose amplitude varies in both time and space as observed in Fig. 3. This is a merit which is absent in the Fourier transform method that assumes implicitly constant amplitude of waves in space and/or time.

As claimed by ECKERMANN and HOCKING (1989), the hodograph analysis, assuming that the wind fluctuations are due to a single monochromatic wave, does not provide accurate estimates of the wave parameters if there exist multiple waves. However, the assumption of monochromaticity is considered to be valid in this study, since the wave structure was extracted using filters, and the fitting was made in a small height region of 1.65 km. The validity is further confirmed by coincident values for a wave parameter (horizontal wavelength) obtained by two independent methods as shown in Section 3.4.

Estimation of wave parameters was made including the effect of vertical shear of the background wind that is not always negligible especially in winter with a strong subtropical jet. HINES (1988) shows that the vertical wind shear can make the hodograph elliptic even for an almost linearly polarized small-scale gravity wave. The dispersion relation and polarization relation for IGW, which are used for the estimation of horizontal wavelength and intrinsic frequency, are modified only through the background wind shear perpendicular to the horizontal wavenumber vector. Taking the horizontal axis in the direction of the horizontal wavenumber vector of the IGW, the modified dispersion relation is

$$\hat{\omega}^2 = f^2 + \frac{N^2k^2}{m^2} - \frac{fV_zk}{m}, \tag{2}$$

and the ratio R of short to long axis of the ellipse derived from the polarization relation becomes

$$R = \frac{f}{\hat{\omega}} - \frac{V_zk}{m\hat{\omega}}, \tag{3}$$

where k, $\hat{\omega}$, V_z, N, and f are the horizontal wavenumber, intrinsic frequency, the background wind shear perpendicular to the direction of k, the Brunt–Väisälä frequency, and the inertial frequency, respectively. The intrinsic frequency $\hat{\omega}$ is taken to be positive without losing any generality. A typical value of 2.09×10^{-2} s^{-1} (corresponding to a period of 5 min) is used as N for the estimation, and f is

8.34×10^{-5} s^{-1} at the MU radar site. The validity of the assumption that $k^2 \ll m^2$ made in equation (2) will be confirmed later. It is also worth noting that only the background horizontal wind U parallel to the horizontal wavenumber vector is important in the following Doppler relation between intrinsic and ground-based frequencies

$$\omega_{obs} = \hat{\omega} + Uk. \tag{4}$$

This equation is used for the estimation of the ground-based phase velocity that will be examined in Section 4.2.

The direction of vertical energy propagation of an IGW is determined by the rotation of the hodograph ellipse: clockwise (anti-clockwise) rotation with altitude shows upward (downward) propagation. The horizontal direction of wave energy propagation relative to the background wind is coincident with the direction of the horizontal wavenumber vector. The horizontal wavenumber vector is parallel to the long axis of the hodograph ellipse, and its direction is determined by the phase difference between the vertical perturbation velocity and the horizontal perturbation velocity parallel to the long axis, using the characteristic of IGWs that the horizontal and vertical perturbation velocities are in phase (out of phase) when the vertical energy propagation is upward (downward).

3.3. *Direction of propagation*

For the direction of vertical energy propagation of IGWs, a distinct seasonal dependence is not seen, in accordance with previous case studies: in all seasons more than 90% of IGWs propagate energy upward in the 14–22 km region of the lower stratosphere. The ratio of upward energy propagation is relatively smaller (but larger than 80%) in the 12–14 km region which is sometimes in the troposphere. The result implies that the source of most of the IGWs is in the troposphere.

Figure 6 presents the percentage of waves propagating energy (relative to the background wind) to the horizontal direction of each sector, in (a) winter and (b) summer as a function of height. The numbers at the bottom of each circle show the total number of IGWs used for the calculation. However, only one tenth of the total waves are independent, because a lowpass filter was used to extract the IGW components as mentioned in Section 2.

In winter IGWs propagate generally southward in the 12–18 km region, while westward IGWs are dominant at 18–22 km. This feature is consistent with the vertical momentum flux shown in Fig. 5, i.e. $\overline{v'w'} < 0$ and $\overline{u'w'} > 0$, since most of the IGWs carry energy upward. In summer northward IGWs are dominant in 18–22 km, whereas there is no systematic anisotropy of propagation direction between 12 and 18 km.

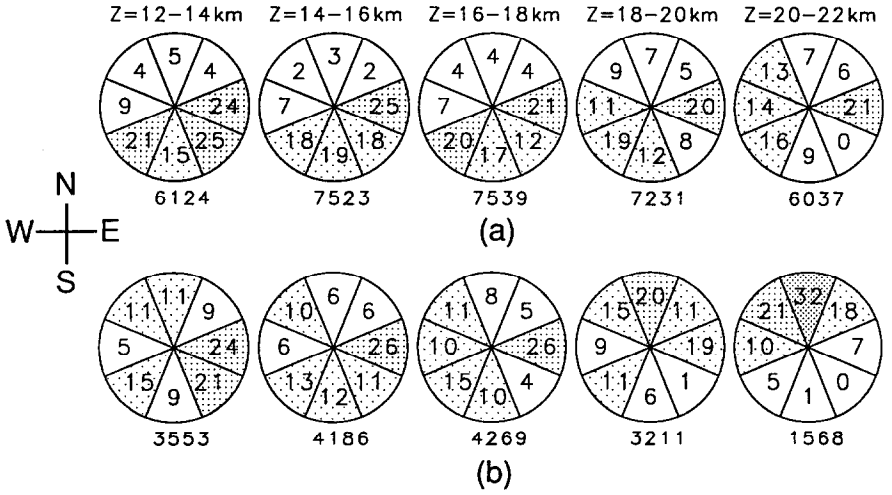

Fig. 6. The distribution of the propagation directions of IGWs in (a) winter and (b) summer at five height regions of 12–14, 14–16, 16–18, 18–20, and 20–22 km. The top, right, bottom, and left sectors show the northward, eastward, southward, and westward propagations, respectively. The number in each sector shows the percentage of the number of IGWs propagating to the direction. The number under each circle denotes the total number of IGWs used for the analysis.

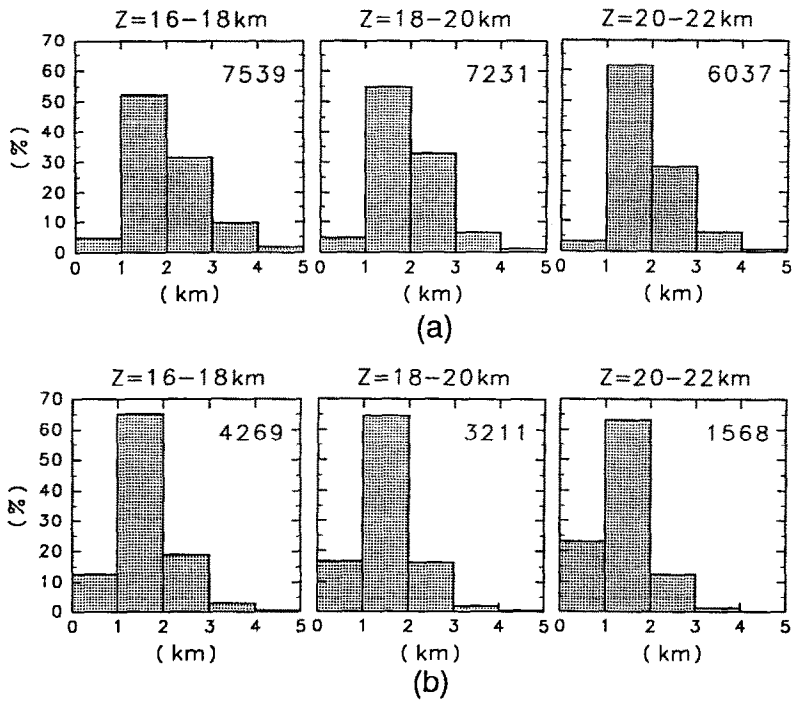

Fig. 7. Histograms of the vertical wavelengths of IGWs in (a) winter and (b) summer for the three height regions of 16–18, 18–20, and 20–22 km. The number in each figure shows the total number of IGWs used for the analysis.

The corresponding positive $\overline{v'w'}$ is not observed in Fig. 5, however.

3.4. *Vertical and horizontal wavelengths and intrinsic period*

Statistics of parameters of the wave structure are shown in this section only for the height region above 16 km, because lower heights are not always in the stratosphere. Figure 7 shows histograms of the vertical wavelengths of IGWs. It is found that the vertical wavelengths in winter are generally larger than in summer. This difference is also observed in the typical wind profiles in Fig. 1. An interesting feature seen in both seasons is that the vertical wavelengths become shorter as the altitude increases. The vertical wavelength averaged for the 16–22 km height region is 2.0 km in winter and 1.6 km in summer.

The propagation direction and vertical wavelength mentioned above are directly obtained by the results of hodograph fitting. The estimation error for the horizontal wavelength, however, is considered not to be small because there are three quantities in equations (2) and (3), m, V_z and R, that should be determined by observations. Thus the horizontal wavelength is examined on a log scale. The results is shown in Fig. 8. A strong dependence on height and season is not observed in the distribution of horizontal wavelengths. Most IGWs are distributed in a range of horizontal wavelengths of 200–500 km and there are few IGWs with wavelengths shorter than 20 km or longer than 1000 km. The average horizontal wavelength is about 300 km.

The horizontal wavelength can be estimated also from the ratio between the amplitudes of horizontal and vertical perturbation velocities, independently of the above method using equations (2) and (3). This method uses the continuity equation under the Boussinesq approximation,

$$ku'_k + mw' = 0, \tag{5}$$

where u'_k is the horizontal perturbation velocity in the direction of the horizontal wavenumber vector. Horizontal wavelengths obtained with this method accord well with those estimated using equations (2) and (3), to within 10–20%. This accordance supports the validity of the monochromatic wave assumption and the accuracy of the parameter estimation. Moreover, it is worth noting that the aspect ratio m/k of

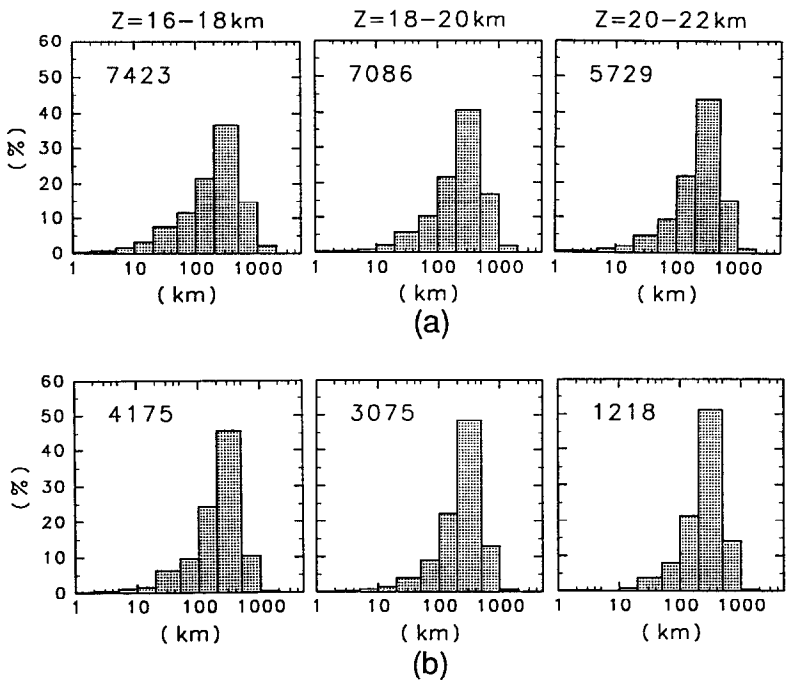

Fig. 8. The same as Fig. 7 but for the horizontal wavelength.

IGWs is about 100, which is consistent with the assumption made in equation (2).

In order to examine the importance of the background wind shear, the horizontal wavelength is estimated by the usual hodograph analysis ignoring the shear effect. For summer similar horizontal wavelengths of about 300 km are obtained but, in winter, in the 16–20 km height region, which has a large background wind shear, the estimated horizontal wavelengths are about 400 km on the average, which is longer by 30–40% than that estimated by the hodograph analysis including the shear effect and that by using the continuity equation. Thus, the effect of the vertical shear of the background wind is not negligible at least in winter.

The distribution of the intrinsic period of IGWs is examined in terms of $f/\hat{\omega}$. This parameter is equal to the ratio R of the short to long axis of the hodograph ellipse when the background wind shear perpendicular to the horizontal wavenumber vector is negligibly weak [see equation (3)]. Thus, for IGWs in summer when the background wind shear is weak and for IGWs propagating zonally in winter when the background wind shear is almost zonal, the estimation of the intrinsic period is more direct and accurate than that of the horizontal wavelength. Figure 9 shows the results. Intrinsic periods ($2\pi/\hat{\omega}$) in summer are nearer to the inertial frequency than in winter and become longer as the altitude increases, while the dependence on altitude is not so strong in winter. The dependence both on season and on altitude is opposite to the tendency for the vertical wavelength, as expected for IGWs with a constant k from the dispersion relation (2).

The average $f/\hat{\omega}$ for the whole 16–22 km height region in the lower stratosphere is 0.47 in winter and 0.54 in summer. For inertio-gravity waves having such a large $f/\hat{\omega}$, the contribution of heat flux to the vertical component of Eliassen–Palm (EP) flux cannot be ignored. The vertical component of EP-flux due to an inertio-gravity wave including the heat-flux term is $[1-(f/\hat{\omega})^2]\overline{u'w'}$ (MIYAHARA *et al.*, 1986). Therefore the drag due to the breaking of IGWs with an average $f/\hat{\omega}$ of about 0.5 is a few tens of percent smaller than the estimation by equation (1) in Fig. 5, when we regard it as the drag for 'zonal-mean' zonal wind.

3.5. *Degree of saturation*

Next the intensity of IGWs is examined in terms of the degree of saturation. LINDZEN (1981) considered that when the amplitude of the horizontal wind component of a monochromatic gravity wave $|u_k'|$ becomes larger than the magnitude of the intrinsic horizontal phase velocity $|\hat{c}|$, breaking of the gravity wave occurs

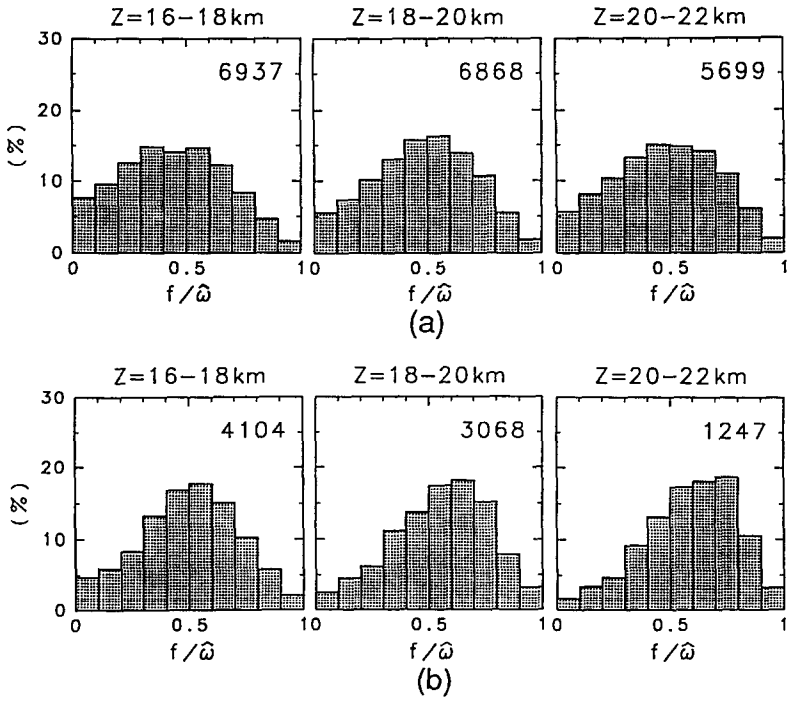

Fig. 9. The same as Fig. 7 but for $f/\hat{\omega}$.

by convective instability so as to make $|u_k'|$ adjusted to $|\hat{c}|$. Such a wave with an amplitude of $|u_k'| = |\hat{c}|$ is called a 'saturated' gravity wave.

The effect of the superposition of waves was considered by SMITH *et al.* (1987) in terms of vertical wavenumber spectra. They showed that the level of vertical wavenumber spectra of the horizontal wind fluctuations $P_v(m)$ can be determined if the spectral shape is known. The observed shape of the spectra is usually proportional to m^{-3} as mentioned in Section 2, resulting in

$$P_v(m) = \frac{1}{6} \times \frac{N^2}{m^3}. \tag{6}$$

From the good agreement between the theory and many observations (TSUDA *et al.*, 1989, 1991), the spectral model of saturated gravity waves proposed by Smith *et al.* has been widely accepted.

On the other hand, there are only a few observational studies that show the saturation of monochromatic gravity waves in the middle atmosphere by comparing $|\hat{c}|$ and $|u_k'|$ directly (e.g. FRITTS, 1984). In this study a statistical examination is possible about the saturation of monochromatic IGWs using parameters obtained by the hodograph analysis. Since IGWs are most dominant in the lower stratosphere, breaking must cause a significant effect on the background wind system.

The ratio of $|u_k'|$ to $|\hat{c}|$ is defined as the degree of saturation S, namely,

$$S = \frac{|u_k'|}{|\hat{c}|}. \tag{7}$$

For a monochromatic saturated gravity wave S becomes one. The normalized distribution of IGWs is shown vs $|u_k'|$ and $|\hat{c}|$ at all heights from 16 to 22 km in Fig. 10. A dashed line denoting $S = 1$ is added for comparison and the dotted line shows the average of S (S_{ave}) for each season. The distribution is not uniform and is elongated along the dotted line in both seasons except for the large phase velocity region ($|\hat{c}| > 7$ m s^{-1}). The average S_{ave} is 0.54 in winter and 0.45 in summer. This difference means that IGWs interact with the background wind more effectively in winter than than in summer, and this reflects the fact that the drag shown in Fig. 5 is larger in winter. Note also that IGWs with large amplitudes of $|u_k'|$ in winter have large intrinsic horizontal phase speeds $|\hat{c}|$, resulting in a small difference in S_{ave} between winter and summer.

Another important point observed for winter is that $|u_k'|$ never seems to be larger than the saturation value

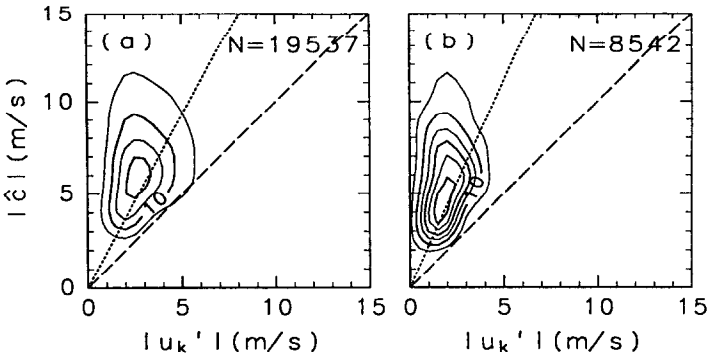

Fig. 10. The distribution of IGWs in a section of the amplitude of horizonal perturbation velocity in the propagation direction ($|u_k'|$) and the intrinsic horizontal phase velocity ($\hat{c}$). The contour interval is 5, but the unit of the contour is arbitrary.

shown by the dashed line. The outer contour of 5 in Fig. 10 is almost parallel to the line of $S = 1$ at smaller $|\hat{c}|$s, in particular. Over-saturated IGWs with $S > 1$ are 5% of the total in winter. The averaged S for the over-saturated IGWs is, however, 1.1, which is considered to be unity within the estimation error. It is concluded, therefore, that the Ss of IGWs in the lower stratosphere are smaller than or equal to unity. This observational fact is consistent with the gravity wave breaking hypothesis of Lindzen. The above results on saturation as well as the parameters describing wave structure are summarized in Table 1.

4. SOURCES

It is considered that the sources of IGWs are related to the subtropical westerly wind jet, since the seasonal variation of the intensity of IGWs is similar to that of the subtropical jet as observed in Fig. 4. The generation mechanisms of IGWs in the lower stratosphere, however, have not been fully understood yet. Hence two analyses for the mechanisms are made in this section.

4.1. *Geostrophic adjustment of the subtropical westerly wind jet*

According to several previous case studies (e.g. HIROTA and NIKI, 1986; YAMANAKA *et al.*, 1989) IGWs in the lower stratosphere prefer meridional propagation as well as in the mesosphere and lower thermosphere (e.g. MEEK *et al.*, 1985; VINCENT and FRITTS, 1987). The result of Section 3.3 indicates that most IGWs propagate southward in the 12–18 km height region in *winter* when the subtropical jet is strong. Thus it might be considered that IGWs are generated due to the geostrophic adjustment process of the subtropical jet elongated zonally. Previous studies indicate that large ageostrophic components are seen in an area across the subtropical jet (e.g. CAMMAS and RAMOND, 1989).

The location of the subtropical jet relative to the MU radar site is an important parameter for examination of the possibility of the geostrophic adjustment process. Figure 11 shows a time–latitude section of the mean horizontal wind velocity at 200 hPa (~12 km) at the longitude of the MU radar (135°E),

Table 1. The wave parameters of inertio-gravity waves in the lower stratosphere

	Summer	Winter
Vertical propagation	Upward	
Horizontal propagation	Northward (z = 18–22 km) No preferred direction (z < 18 km)	Westward (z = 18–22 km) Southward (z = 12–18 km)
Vertical wavelength	1.6 km	2.0 km
	Decreases with altitude	
Horizontal wavelength	~300 km	
$f/\hat{\omega}$	0.54	0.47
	Increases with altitude	Almost constant
Degree of saturation	0.45	0.54

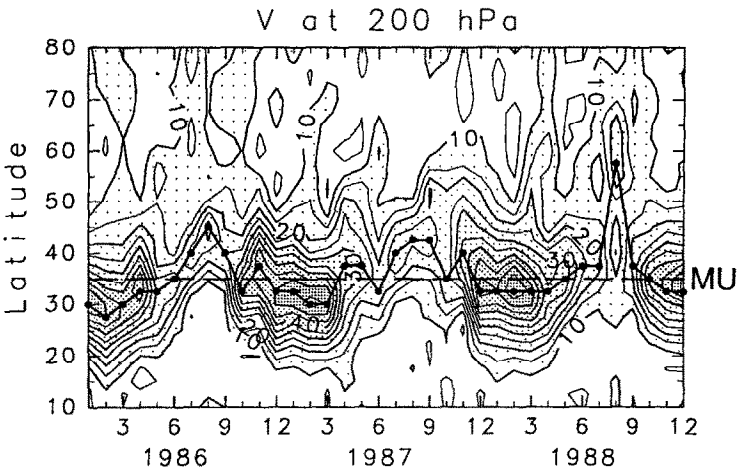

Fig. 11. A time–latitude section of the absolute value of the horizontal wind velocity vector at a longitude of 135°E at 200 hPa. The small dots connected with solid lines show the latitudes of the maximum in each month. The dashed line shows latitude of the MU radar site.

made using ECMWF operational data distributed at intervals of 2.5° in both latitude and longitude and 12 h in time. The level of 200 hPa roughly corresponds to the altitude of the wind maximum of the subtropical jet. The profile for each month was obtained by averaging for one week around the period of the MU radar observations. The solid thick curve traces the latitude of the maximum of the horizontal wind in each month and the dashed line is at the latitude of the MU radar site.

The axis of the subtropical jet is usually located south of the MU radar site in winter. Comparison with Fig. 6 indicates that the IGWs at heights of 12–18 km in winter propagate energy *toward* the latitude of the jet axis. The jet position is not always steady during each observation time of 100 h. The relative position of each IGW is determined with a resolution of 4 km in height and 2.5° in latitude by using the original wind data of ECMWF with a time interval of 12 h, and the averaged energy propagation direction at each relative latitude and altitude is obtained. The result for winter is shown in Fig 12(a). The half width of the jet is roughly shown by the dotted ellipse. The length p of the upward component of the arrow indicates that $50(1+p)\%$ of IGWs propagate energy upward. The length of the rightward arrow q shows the average of meridional projection of the horizontal wavenumber vector normalized by the absolute horizontal wavenumber, indicating that $50(1+q)\%$ of IGWs propagate northward. The unit vectors on the

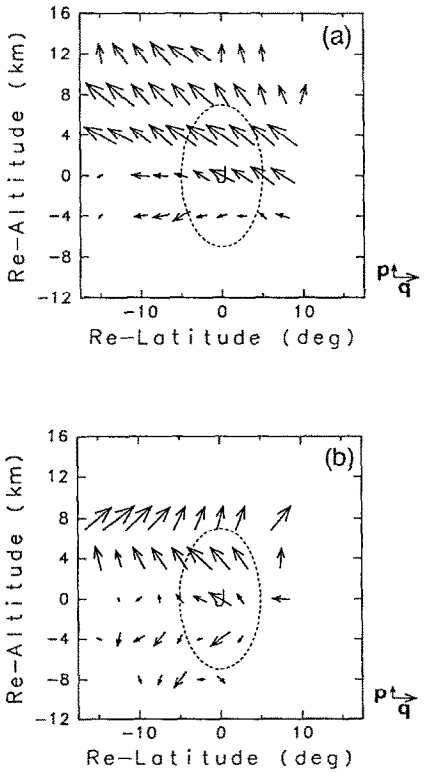

Fig. 12. The propagation direction of IGWs in the section of latitude and altitude relative to the axis of the subtropical jet for (a) winter and (b) summer. The dotted ellipse shows roughly a region with a half strength of the jet.

right-hand side of the panels show lengths of $p = 0.5$ (75% upward) and $q = 0.5$ (75% northward), respectively. Arrows were plotted only for positions where the number of IGWs exceeds 200.

IGWs south of the jet axis propagate southward, i.e. outward from the jet axis. The vertical propagation directions of the IGWs are upward and downward from the altitude of the jet. These features are consistent with gravity wave generation due to the geostrophic adjustment process around the jet axis. In the north part of the jet where a large number of IGWs are distributed, however, IGWs also propagate southward, i.e. *toward* the latitude of jet. The ratio of southward propagating waves is larger than 75%, which is a strong anisotropy since the normalization of p was made with the absolute horizontal wavenumber vector including the zonal component. This feature also holds for an analysis including a time-lag between the IGWs and the jet.

There is a case study made by HIROTA and NIKI (1986) in terms of the relation between IGWs and the westerly jet using the MU radar data. From the result obtained by a hodograph analysis that IGWs propagated upward and downward from the altitude of the wind maximum of the subtropical jet, they inferred that the jet is a source of IGWs. The phase difference between the horizontal and vertical perturbation velocities, however, indicated that IGWs propagate *toward* the latitude of the jet axis, although that was not specified in the paper. The meridional propagation was not consistent with the generation around the jet axis, either.

It is deduced, therefore, that most IGWs propagating meridionally in winter which are mainly observed at heights of 12–18 km (above the ground) are not generated by the geostrophic adjustment process, at least just at the jet axis.

Results for summer are presented in Fig. 12(b) for comparison, because a weak subtropical jet also exists in this season. The IGWs 4 km above and to the south of the jet axis propagate southward although the anisotropy is not as strong as in winter. It is important that there are height regions 8 km above the jet axis which are occupied by IGWs propagating northward from the south of jet. This feature is also not consistent with a view of wave generation due to the geostrophic adjustment process at the jet axis.

4.2. *Topographic forcing*

One possible local generation mechanism of IGWs in the lower stratosphere is the topographic effect because the surface wind is strongest in winter when the subtropical jet is most intensive. Figure 13 shows

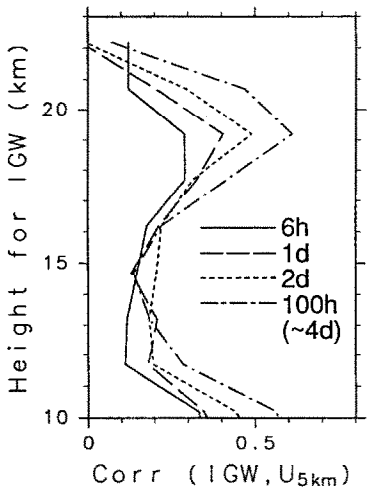

Fig. 13. The correlation between the r.m.s. of horizontal perturbation velocities $\sqrt{\overline{u'^2+v'^2}}$ of IGWs and the magnitude of the background horizontal wind at the lowest altitude (~5 km) observed by the MU radar. Different type of line shows the results of different time interval for the calculation of r.m.s. of the horizontal perturbation velocities.

the correlation in winter between the root-mean-square (r.m.s.) of horizontal perturbation velocities of IGWs and the magnitude of the horizontal background wind at about 5 km, which is the lowest altitude observed by the MU radar. The different lines show the results of different averaging times used for calculation of the r.m.s. A high correlation, more than 0.6, is found between the low level wind and the r.m.s. of IGWs around an altitude of 19 km for an averaging time of the whole observation period of each month, although the correlation becomes lower as the averaging time decreases. Thus it is possible that IGWs around 19 km are controlled by the *local* wind at lower levels in winter.

Mountain waves possibly have short vertical wavelengths similar to IGWs in the lower stratosphere where the background wind is weak and N is almost twice as large as that in the troposphere. Moreover, it is considered that the geographical position of the spatial phase of mountain waves changes slowly in the slowly varying background wind, so that mountain waves are observed at a single site by the MU radar as waves whose vertical structure varies slowly as IGWs. The large negative $\overline{u'w'}$ in winter is consistent with the characteristics of mountain waves generated in the strong westerly wind near the surface which is dominant in winter around Japan.

It has been known that intense mountain waves frequently appear as vertical wind disturbances over the MU radar site from late autumn to early spring

(SATO, 1990). The possibility of generation by topographic forcing is further examined by comparing the characteristics of IGWs in two kinds of month in winter, categorized by the existence of vertical wind disturbances. First, the mean square of vertical winds in the 5–20 km height region, $\overline{w'^2}$, is obtained for each month. Next, the months with $\overline{w'^2}$ larger than a threshold value of $0.16\ m^2\ s^{-2}$ are defined as MW periods (with mountain waves) and the others as NMW periods (with no mountain waves). The threshold value is taken following SATO (1990). Comparison is made between MW and NMW periods having a maximum of 60–80 $m\ s^{-1}$ in the vertical profile of the background wind, in order to make the background conditions for gravity wave propagation equal. The number of months belonging to the MW and NMW periods are 6 and 5, respectively. Figure 14 shows vertical profiles of the background wind, vertical momentum flux, variance, and drag to the background wind, averaged for MW and NMW periods, respectively. The variance around 20 km where the correlation with the low-level wind is high (Fig. 13) is larger in the MW period than in the NMW period, whereas there is no distinct difference in the variance around 16 km between the two periods, suggesting a connection between IGWs around 20 km and mountain waves. It is also important that the values of $\overline{u'w'}$ increase with height over the large region from 19 to 23 km in the MW period, corresponding to a large westward drag of 3–5 $m\ s^{-1}\ day^{-1}$. Both the variance and momentum flux become zero at heights where the background wind is nearly zero, which is consistent with characteristics at a critical level of mountain waves. Note that these features are not observed in the NMW period around a height of 20 km where the background wind is also weak.

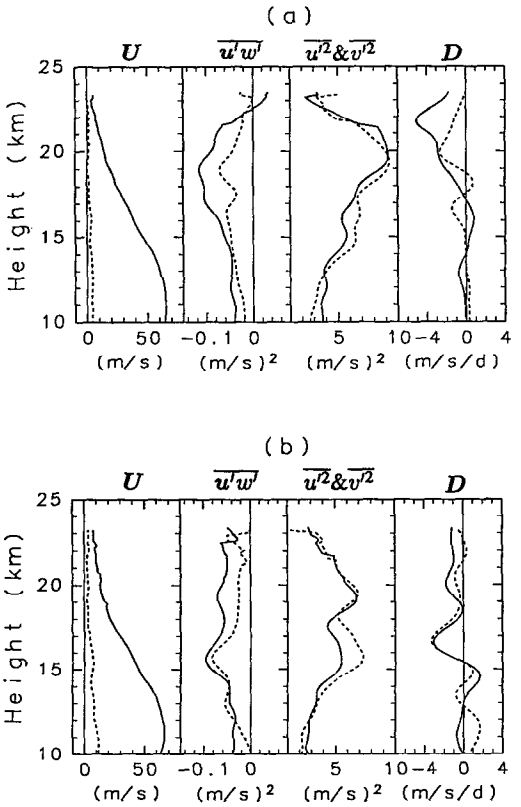

Fig. 14. The same as Fig. 5 but for the (a) MW and (b) NMW period in winter.

Horizontal energy propagation directions relative to the background wind in MW and NMW periods are shown in Fig. 15(a) and 15(b), respectively. Westward IGWs in the 18–22 km height region are observed only in MW periods whereas southward IGWs at 12–18 km are observed similarly in both periods. This westward propagation relative to the background wind is also in accord with the characteristics of mountain waves.

Finally, we examine the ground-based phase velocity, c_{obs}, which must be almost zero if the IGWs are due to mountain waves. Figure 16 shows the histogram of the ground-based phase velocity of IGWs propagating westward, northwestward, and southwestward relative to the background wind in the 18–22 km height region which are obtained using equation (4). It is very clear that the ground-based phase velocities are distributed around zero.

Therefore, it is highly possible that the IGWs observed at heights of 18–22 km in winter, which are most dominant in the seasonal cycle, are due to mountain waves. On the other hand, the possibility of mountain waves for meridionally propagating IGWs observed at 12–18 km in winter is questionable since the meridional background wind is not biased strongly enough to produce such a strong anisotropy of meridional propagation of IGWs.

It is noteworthy that the vertical profiles of $\overline{u'^2}$ and $\overline{u'w'}$ shown in Fig. 5(a) are similar to those of the MW period in Fig. 14 in shape above 20 km. Thus the large drag observed in winter above 20 km can be considered to be due to the breaking of mountain waves approaching a critical level. Severe mountain waves as examined by LILLY and KENNEDY (1973) and SATO (1990) are not always present and occur rather sporadically (e.g. SATO, 1990). In fact, large variances and momentum fluxes are observed only in MW periods and not in NMW periods. This is the reason why the magnitude of $\overline{u'w'}$ in winter that is

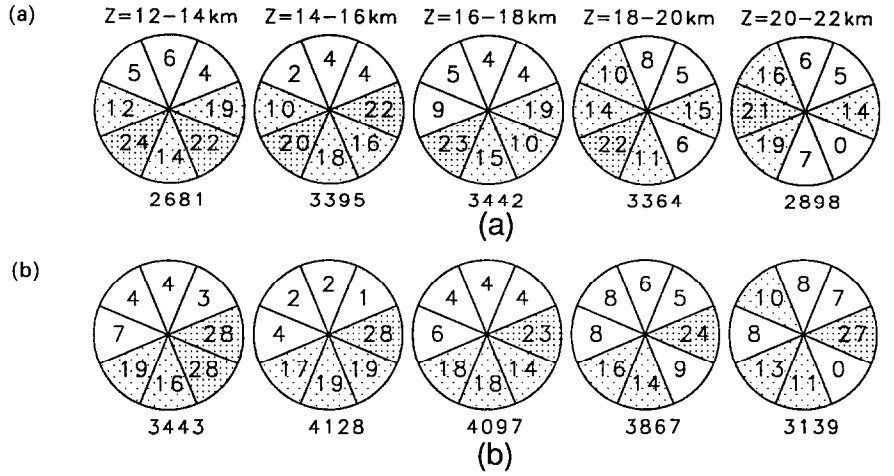

Fig. 15. The same as Fig. 6 but for the (a) MW and (b) NMW period in winter.

obtained statistically in Section 3.1 is a few tens of percent of that of typical severe mountain waves.

5. DISCUSSION

5.1. *Wave parameter dependence on season and altitude*

HIROTA and NIKI (1985) examined the seasonal variation of $f/\hat{\omega}$ of IGWs in the 30–60 km height region using rocket data. Although the assumption of monochromatic waves made in their analysis may not always hold as noted by ECKERMANN and HOCKING (1989), the result that the distribution of $f/\hat{\omega}$ is independent of season still implies a wide range of ground-based horizontal phase velocities of the IGWs. The dependence on season of $f/\hat{\omega}$ in the upper stratosphere contrasts with that obtained in this study for the lower stratosphere. The difference between summer and winter is rather consistent with the characteristic of (quasi)-stationary gravity waves with constant k, that $f/\hat{\omega}$ is proportional to the inverse of the background wind. In fact, it was shown in the previous section that intense IGWs around 20 km in winter have almost zero ground-based horizontal phase velocities. Moreover, the coincidence of altitudes where $\overline{u'w'}$ and the background zonal wind become zero in summer as observed in Fig. 5(b) suggests that IGWs have ground-based horizontal phase velocities distributed around zero.

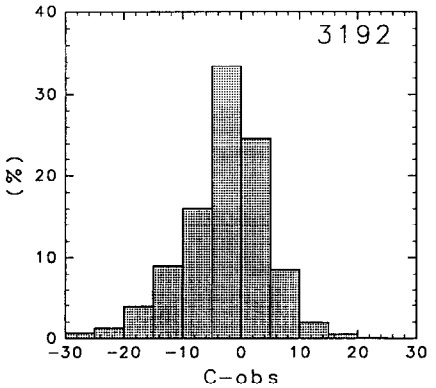

Fig. 16. The distribution of the ground-based horizontal phase velocity of IGWs propagating westward, northwestward and southwestward in the 18–22 km height region in the MW periods.

The wave parameters were sensitive to altitude as well as to season in the lower stratosphere. For example, the vertical wavelength becomes shorter as the altitude increases in both summer and winter seasons. The dependence is very simple; the interpretation is difficult, however. The horizontal energy propagation directions of IGWs are not constant in the lower stratosphere, as found in Section 3.3, indicating that the direction of the background wind that affects the IGW vertical wavelength through Doppler shifting of the intrinsic frequency depends on height. Thus we cannot interpret the vertical wavelength tendency simply with the Doppler effect by the background wind whose vertical profile itself is simple.

It may be possible to interpret the dependence of the vertical wavelength on altitude in winter using the spectral theory of saturated gravity waves by SMITH *et al.* (1987), which predicts that the characteristic vertical wavenumber becomes smaller as the total kinetic energy divided by the air density (and hence the total variance of horizontal wind fluctuations to a

good approximation) of gravity waves increases, since the vertical wavenumber spectrum in winter was found to be saturated (TSUDA *et al.*, 1991). The theory explains well the difference in characteristics, that is, the dominant vertical wavenumber among large-scale height regions of troposphere, stratosphere, mesosphere, etc. The same theory predicts for the lower stratosphere that the total horizontal wind variance would decrease with altitude if the vertical wavenumber tended to increase with altitude as found in this study.

The vertical profile of density-weighted total variance of wind fluctuations with ground-based frequencies between f and N was examined recently by MURAYAMA *et al.* (1993). A variance decrease with altitude was observed but it was almost as large as explained by the air density decrease with altitude. It should be noted that the variance obtained by Murayama *et al.* does not include quasi-stationary gravity waves like mountain waves having ground-based frequencies lower than f. This study shows that quasi-stationary mountain waves are dominant at least in winter around a height of 20 km, and that there is no clear tendency to decrease with height also for the variance of IGWs including mountain waves (Fig. 5). Though there may be other gravity waves with frequencies largely Doppler-shifted by the strong background wind, it is difficult to identify such gravity waves, at least using data from a single site observation. Thus, further investigation is not possible from the viewpoint of the spectral theory.

5.2. *Implications of the seasonal dependence of IGW intensity*

Next let us consider why the amplitude of IGWs is larger in winter than in summer. As mentioned above, IGWs having nearly zero ground-based horizontal phase velocities are dominant in both seasons in the lower stratosphere. Their intrinsic phase velocities must be larger in winter since the background wind is strong. This is the case as shown in Section 3.5. The intrinsic phase velocity gives the upper limit to the amplitude of the horizontal perturbation velocity of an IGW. Thus, one of the reasons for the large amplitude of horizontal perturbation velocity in winter is considered to be the strong background wind.

It can be shown further that the activity of IGW sources is also important for the difference in amplitude as follows. If the strength of sources of IGWs were constant throughout the year, the drag due to IGW breaking would be larger in summer since the breaking of IGWs occurs more effectively in the weak background wind. The observational fact shows, however, that this is not the case. This indicates that the IGW sources are more active in winter. In fact the surface wind over the mountains which is one of the sources of IGWs is strong in winter.

5.3. *Localization of IGWs*

An important result of this study is that some intense IGWs in the lower stratosphere are likely to be mountain waves. This indicates the possibility that IGWs in the lower stratosphere are distributed depending on local topography.

KITAMURA and HIROTA (1989) examined the latitudinal distribution of disturbances, which are considered to be due to IGWs, by projecting longitudinally the radiosonde data at eight stations over Japan and showed that the IGWs in the lower stratosphere are most intense in winter in a latitudinal region of 5–10° north of the subtropical jet axis. It was also shown by examining the phase difference between the fluctuations of temperature and the horizontal wind vector that the intense IGWs propagate energy northwestward (relatively to the background wind), which is outward from the jet stream. However, the distribution may reflect the localization. For example, let us consider the IGWs observed in Akita, which is one of the stations where the IGW intensity is large and which is located windward of mountains in winter. A sonde launched at Akita station moves leeward in the strong westerly background wind by a horizontal distance of about 70–100 km when it reaches the altitude region of 15–20 km in which IGWs were dominant. Since there are mountains with altitudes of about 1500 m located at a 20 km distance from Akita, the sonde possibly observes the mountain waves. The northwestward energy propagation direction of IGWs relative to the background wind is also consistent with this speculation. Further analysis is necessary using data from many stations to examine the latitudinal distribution of IGWs.

5.4. *Long horizonal wavelength of mountain waves*

While horizontal wavelengths of mountain waves observed in the troposphere are usually only some tens of kilometers, the IGWs in the lower stratosphere considered to be mountain waves have long wavelengths of about 300 km. This may be explained by the difference in vertical transmission of mountain waves depending on the horizontal wavelength. Mountain waves with short horizonal wavelengths do not propagate energy upward in a strong background wind, since the Scorer parameter, which is an index of characteristics of vertical propagation of gravity waves and corresponds to the square of the vertical

wavenumber under the WKB approximation (e.g. HOLTON, 1992), is negative. For example, mountain waves with horizontal wavelengths less than about 50 km cannot propagate upward through the jet structure of background wind with a maximum of 80 m s^{-1}.

6. SUMMARY AND CONCLUDING REMARKS

Using wind data obtained by the MU radar in the three years of 1986–1988, a statistical analysis was made on the structure, saturation, and sources of IGWs with periods longer than 10 h and vertical wavelengths shorter than 4 km observed in the lower stratosphere in all seasons.

An annual cycle with a maximum in winter is dominant in the seasonal variation of IGW intensity. The zonal component of vertical momentum flux $\overline{u'w'}$ is mostly negative in winter and almost zero in summer.

By analyzing hodographs of IGWs in the lower stratosphere, a statistical description was made of the characteristics on the wave structure and saturation, comparing two seasons of winter with a strong subtropical jet and summer with a weak jet.

1. Strong anisotropy of horizontal energy propagation direction relative to the background wind is observed: this is southward at heights of 12–18 km and westward at 18–22 km in winter; and northward around 20 km in summer. More than 90% of IGWs propagate energy upward.

2. The horizontal wavelengths are distributed in a range of 200–500 km, independent of season and altitude. The vertical wavelengths are about 2 km, smaller in summer than in winter, and smaller as the altitude increases. The parameter $f/\hat{\omega}$ is about 0.5 in average, larger in summer than in winter, and larger as the altitude increases (not clear in winter). These results about wave structure are in harmony with the dispersion relation of IGWs.

3. The degree of saturation is larger in winter than in summer. There are few over-saturated IGWs even in winter.

The subtropical westerly wind jet is strong over the MU radar site in winter when intense IGWs are observed. An analysis was made of two possibilities of generation mechanisms related to the strong jet, namely, the geostrophic adjustment process and the topographic effect. By examining the meridional propagation direction of IGWs in a section of latitude and altitude relative to the axis of subtropical westerly wind jet with the aid of wind data from ECMWF, it was found that most of the IGWs observed at heights of 12–18 km (above the ground) in winter are situated in the north of jet axis and propagate southward, namely, toward the latitude of the jet axis. Similarly the IGWs at 18–22 km in summer propagate northward and toward the jet axis from the south of the jet. This fact shows that the geostrophic adjustment process just *at* the jet axis is not the dominant generation mechanism of these IGWs.

The characteristics of the most intense IGWs observed at 18–22 km in winter, on the other hand, accord well with mountain waves: westward propagation relative to the background wind; large and negative $\overline{u'w'}$; almost zero ground-based phase speed; vertical profiles of variance and momentum flux consistent with the feature near a critical level of mountain waves.

Sources of IGWs propagating southward in the 12–18 km height region in winter and propagating northward in 18–22 km in summer are remaining issues. It was shown that they are not generated due to geostrophic adjustment just at the axis of the subtropical jet, as is considered using a numerical model by FRITTS and LUO (1992). Topographic forcing is also hard to be considered as a generation mechanism for the IGWs as discussed in the last part of Section 4.2. However, it is possible that geostrophically unbalanced regions related to gravity wave generation concentrate to the north of the jet axis. According to CAMMAS and RAMOND (1989), ageostrophic components are observed in a wide area of $\sim$1000 km across the subtropical jet even in summer. The large-scale background wind structure must be investigated in detail. One possible excitation mechanism of the IGWs in summer is convection in the ITCZ as is discussed by USHIMARU and TANAKA (1990). It is necessary to make further examinations from this viewpoint.

Acknowledgments—The author would like to thank I. Hirota for his fruitful discussion and comments, and T. Sato for his useful discussion. Thanks are also extended to two anonymous reviewers for their valuable comments, and to the regional editor, T. E. VanZandt, for his critical reading of the manuscript and comments. The MU radar belongs to and is operated by the Radio Atmospheric Science Center of Kyoto University.

REFERENCES

CADET D. and TEITELBAUM H. 1979 Observational evidence of internal inertio-gravity waves in the tropical stratosphere. *J. atmos. Sci.* **36**, 892–907.

CAMMAS J. P. and RAMOND D. 1989 Analysis and diagnosis of the composition of ageostrophic circulations in jet-front systems. *Mon. Weath. Rev.* **117,** 2447–2462.

CORNISH C. R. and LARSEN M. F. 1989 Observations of low-frequency inertia-gravity waves in the lower stratosphere over Arecibo. *J. atmos. Sci.* **46,** 2428–2439.

EBEL A., MANSON A. H. and MEEK C. E. 1987 Short period fluctuations of the horizontal wind measured in the upper middle atmosphere and possible relationship to internal gravity waves. *J. atmos. terr. Phys.* **49,** 385–401.

ECKERMANN S. D. and HOCKING W. K. 1989 The effect of superposition on measurements of atmospheric gravity waves: a cautionary note and some reinterpretations. *J. geophys. Res.* **94,** 6333–6339.

FRITTS D. C. 1984 Gravity wave saturation in the middle atmosphere: a review of theory and observations. *Rev. Geophys. Space Phys.* **22,** 275–308.

FRITTS D. C. and LUO Z. 1992 Gravity wave excitation by geostrophic adjustment of the jet stream, Part 1: two-dimensional forcing. *J. atmos. Sci.* **49,** 681–712.

FRITTS D. C., TSUDA T., SATO T., FUKAO S. and KATO S. 1988 Observational evidence of a saturated gravity wave spectrum in the troposphere and lower stratosphere. *J. atmos. Sci.* **45,** 1741–1759.

FUKAO S., TSUDA T., SATO T., KATO S., WAKASUGI K. and MAKIHIRA T. 1985b The MU radar with an active phased array system, 2. In-house equipment. *Radio Sci.* **20,** 1169–1176.

FUKAO S., SATO T., TSUDA T., KATO S., WAKASUGI K. and MAKIHIRA T. 1985a The MU radar with an active phased array system, 1. Antenna and power amplifiers. *Radio Sci.* **20,** 1155–1168.

HINES C. O. 1988 Tropopausal mountain waves over Arecibo: a case study. *J. atmos. Sci.* **46,** 476–488.

HIROTA I. 1984 Climatology of gravity waves in the middle atmosphere. *J. atmos. terr. Phys.* **46,** 767–773.

HIROTA I. and NIKI T. 1985 A statistical study of inertia-gravity waves in the middle atmosphere. *J. met. Soc. Japan* **63,** 1055–1066.

HIROTA I. and NIKI T. 1986 Inertia-gravity waves in the troposphere and stratosphere observed by the MU radar. *J. met. Soc. Japan* **64,** 995–999.

HOLTON J. R. 1992 *An Introduction to Dynamic Meteorology*, Third Edition, 507pp. Academic Press, New York.

IWASAKI T., YAMADA S. and TADA K. 1989 A parameterization scheme of orographic gravity wave drag with two different vertical partitionings, Part 1: impacts on medium-range forecasts. *J. met. Soc. Japan* **67,** 11–27.

KITAMURA Y. and HIROTA I. 1989 Small-scale disturbances in the lower stratosphere revealed by daily rawinsonde observations. *J. met. Soc. Japan* **67,** 817–831.

LILLY D. K. and KENNEDY P. J. 1973 Observations of a stationary mountain wave and its associated momentum flux and energy dissipation. *J. atmos. Sci.* **41,** 1135–1152.

LINDZEN R. S. 1981 Turbulence and stress owing to gravity wave and tidal breakdown. *J. geophys. Res.* **86,** 9707–9714.

LUO Z. and FRITTS D. C. 1993 Gravity wave excitation by geostrophic adjustment of the jet stream, Part 2: three-dimensional forcing. *J. atmos. Sci.* **50,** 104–115.

MANSON A. H. and MEEK C. E. 1986 The dynamics of the mesosphere and lower thermosphere at Saskatoon (52°N). *J. atmos. Sci.* **43,** 276–284.

MEEK C. E., REID I. M. and MANSON A. H. 1985 Observations of mesospheric wind velocities. II. Cross sections of power spectral density for 48–8 h, 8–1 h, 1 h–10 min over 60–110 km for 1981. *Radio Sci.* **20,** 1383–1402.

MIYAHARA S., HAYASHI Y. and MAHLMAN J. D. 1986 Interactions between gravity waves and planetary scale flow simulated by the GFDL 'SKYHI' general circulation model. *J. atmos. Sci.* **43,** 1844–1861.

MURAYAMA Y., TSUDA T. and FUKAO S. 1993 Seasonal variation of gravity wave activity in the lower atmosphere observed with the MU radar. *J. geophys. Res.* (submitted).

PALMER T. N., SHUTTS G. J. and SWINBANK R. 1986 Alleviation of a systematic westerly bias in general circulation and numerical weather prediction models through a gravity wave drag parameterization. *Q. Jl R. met. Soc.* **112,** 1001–1039.

SATO K. 1990 Vertical wind disturbances in the troposphere and lower stratosphere observed by the MU radar. *J. atmos. Sci.* **47,** 2803–2817.

SATO K. 1993 Small-scale wind disturbances observed by the MU radar during the passage of Typhoon Kelly. *J. atmos. Sci.* **50,** 518–537.

SATO T. and WOODMAN R. F. 1982 Fine altitude resolution radar observations of upper tropospheric and lower-stratospheric winds and waves. *J. atmos. Sci.* **39,** 2539–2545.

SMITH S. A., FRITTS D. C. and VANZANDT T. E. 1987 Evidence of a saturation spectrum of atmospheric gravity waves. *J. atmos. Sci.* **44,** 1404–1410.

TSUDA T., INOUE T., FRITTS D. C., VANZANDT T. E., KATO S., SATO T. and FUKAO S. 1989 MST radar observations of a saturated gravity wave spectrum. *J. atmos. Sci.* **46,** 2440–2447.

TSUDA T., MURAYAMA T., YAMAMOTO M., KATO S. and FUKAO S. 1990 Seasonal variation of momentum flux in the mesosphere observed with the MU radar. *Geophys. Res. Lett.* **17,** 725–728.

TSUDA T., VANZANDT T. E., MIZUMOTO M., KATO S. and FUKAO S. 1991 Spectral analysis of temperature and Brunt–Väisälä frequency fluctuations observed by radiosondes. *J. geophys. Res.* **96,** 17,265–17,278.

USHIMARU S. and TANAKA H. 1990 Characteristics of internal inertial gravity waves and inertial waves in the lower stratosphere observed by the MU radar. *J. met. Soc. Japan* **68,** 1–18.

VINCENT R. A. and FRITTS D. C. 1987 A climatology of gravity waves in the mesopause region at Adelaide, Australia. *J. atmos. Sci.* **44,** 748–760.

VINCENT R. A. and REID I. M. 1983 HF Doppler measurements of mesospheric gravity wave momentum fluxes. *J. atmos. Sci.* **40,** 1321–1333.

WILSON R., CHANIN M. L. and HAUCHECORNE A. 1991 Gravity waves in the middle atmosphere observed by Rayleigh lider. Part 2: Climatology. *J. geophys. Res.* **96,** 5169–5183.

YAMAMOTO M., SATO T., MAY P. T., TSUDA T., FUKAO S. and KATO S. 1988 Estimation error of spectral parameters of MST radar obtained by least squares fitting method and its lower bound. *Radio Sci.* **23,** 1013–1021.

YAMANAKA M. D., FUKAO S., MATSUMOTO H., SATO T., TSUDA T. and KATO S. 1989 Internal gravity wave selection in the upper troposphere and lower stratosphere observed by the MU radar: preliminary results. *Pure appl. Geophys.* **130,** 481–495.

APPENDIX

Error in vertical momentum flux of IGWs

The vertical momentum flux is obtained by the method of VINCENT and REID (1983) that provides most accurate estimates for MST radar observations with a five beam configuration:

$$\overline{u'w'} = \frac{\overline{V'^2_{+\theta}} - \overline{V'^2_{-\theta}}}{2 \sin 2\theta}, \tag{A1}$$

where $V'_{\pm\theta}$ are the line-of-sight wind fluctuation components of IGWs observed with a symmetrical beam pair with a zenith angle of θ. The overline denotes a temporal and/or spatial average. When the observed velocities $V'_{\pm\theta}$ are composed of the true value $\tilde{V}_{\pm\theta}$ and the random error of estimation $\delta_{\pm}$,

$$V'_{\pm\theta} = \tilde{V}_{\pm\theta} + \delta_{\pm}, \tag{A2}$$

the estimation error for $V'^2_{\pm\theta}$ is expressed by $2\delta_{\pm}\tilde{V}_{\pm\theta}$ with error $O[\delta^2_{\pm}]$. Thus, assuming $\overline{\delta^2_+} \approx \overline{\delta^2_-} \equiv \overline{\delta^2}$ and $\overline{\tilde{V}^2_{+\theta}} \approx \overline{\tilde{V}^2_{-\theta}} \equiv \overline{\tilde{V}^2_{\theta}}$, variance of the estimation error of vertical momentum flux is given by

$$\sigma^2_{\overline{u'w'}} = \frac{2\overline{\delta^2}\,\overline{\tilde{V}^2_{\theta}}}{(\sin 2\theta)^2} \cdot \frac{1}{N}, \tag{A3}$$

where N is number of data used for the average. The estimation error of the line-of-sight wind velocity of a 1-min observation is about 0.1 m s^{-1} when the signal-to-noise of atmospheric echo is sufficiently high (YAMAMOTO *et al.*, 1988). Since the line-of-sight perturbation velocity of IGWs is obtained using a lowpass filter corresponding to an average

of 120 data points, $\sqrt{\overline{\delta^2}}$ for the present case is about 0.01 $(0.1/\sqrt{120})$ m s^{-1}. The number of average N is 800 (20 in time and 40 in altitude) for Fig. 4. The variance of one horizontal perturbation velocity $\overline{u'^2}$ of IGWs is about 7 m^2 s^{-2} in winter (3 m^2 s^{-2} in summer) as found from Fig. 4, indicating that $\overline{\tilde{V}_\theta^2}$ ($\approx \overline{u'^2} \times \sin^2\theta$) is 0.2 m^2 s^{-2} in winter (0.09 m^2 s^{-2} in summer). Using these values the error of vertical momentum flux ($\sigma_{\overline{u'w'}}$) is estimated to be about 1×10^{-3} m^2 s^{-2} for Fig. 4. Similarly the estimation for the vertical momentum flux in Fig. 5 and Fig. 14 can be made and the errors are found to be of the same order as that for Fig. 4 (the calculation is not shown in detail).